

Seismic Imaging from a TBM

By

G. Swinnen, J. W. Thorbecke, and G. G. Drijkoningen

Faculty of Civil Engineering and Geosciences, Delft University of Technology,
Delft, The Netherlands

Received April 29, 2005; accepted June 14, 2006
Published online December 5, 2006 © Springer-Verlag 2006

Summary

Seismic monitoring from the head of a tunnel-boring machine (TBM) enables improved assessment of the risks associated with the tunnel-boring process. The monitoring system provides a live image of ground conditions along the trajectory followed by the TBM and detects local heterogeneities such as boulders, foundations, and other obstacles that commonly pass undetected using local geotechnical techniques. From a seismic perspective, the underground setting of tunnelling projects places limitations on imaging capability. The principal limiting factor is the size of the area upon which transducers can be installed. This limitation requires adjustments to traditional seismic imaging techniques in which a large area is assumed to be available for attaching the transducers. Recently developed short imaging operators take this limitation into account and are used in the examples described herein. The unique conditions of tunnelling yield two advantages over traditional settings in terms of imaging: rotation of the cutter wheel and the lateral progression of the TBM. Rotation of the cutter wheel, upon which the transducers are installed, provides the opportunity to illuminate obstacles from different angles in different recordings. Spatial progression of the TBM enables improvement in the illumination of obstacles and the signal-to-noise ratio by combining recordings from different lateral positions. In this paper, these specific aspects of seismic imaging during tunnelling are discussed via models that represent different cases encountered in actual tunnelling projects. These case studies demonstrate the way in which image quality along the trajectory of the TBM is improved over that in traditional settings. In this way, the risks associated with the tunnelling process can be more accurately assured.

Keywords: Monitoring, wavefield extrapolation, imaging, tunneling, prediction of ground conditions.

1. Introduction

Tunnel boring in soft soil is a relatively new development that is useful in heavily urbanized areas where boring a tunnel is a good alternative to cut-and-cover excavation. However, buildings and other structures above the tunnel must not be damaged in any way. This requires extra care and additional costs for the tunnel-boring operation.

Commonly, before tunnelling has begun, ground conditions along the tunnel alignment are investigated to plan and fine-tune the boring process. Potential risks of this process are erroneous predictions of ground conditions. For instance, non-detection of sand lenses with high pore-water pressures can lead to the later development of problems such as instability of the tunnel face, damage to structures above the tunnel, and stagnation of the TBM. Other undetected geological features can slow down the tunnelling progress; e.g., peat is difficult to excavate because of its tough structure. Obstacles such as boulders, relic bombs, and the remains of older subsurface constructions that are buried in the path of the TBM are extremely damaging to the TBM because it is designed to bore through soft soils rather than demolish hard obstacles. If obstacles are detected before collision with the TBM, it is possible to remove them or adjust the alignment of the tunnel.

Predictions of ground conditions are based on a combination of different in situ and laboratory tests. Cuttings washed from the borehole via the boring fluid provide a rough indication of soil type. The analysis of soil samples provides information on the grain-size distribution, organic content, colour, water content, and density of the soil. Undisturbed samples are analysed in the laboratory to determine the stress-strain response of the soil and its hydraulic properties. Cone penetration tests (CPTs) or soundings yield local in situ information, and are usually performed at 25–50 m intervals to provide vertical profiles at each analysis site. Sensors within boreholes (e.g., piezometers, extensometers, and inclinometers) can also be used to monitor the dynamics of the soil, thereby ensuring geotechnical control of the boring process.

Borings and soundings are performed slightly offset from the alignment of the tunnel (Wermer, 1997) to prevent disturbance of the soil above the tunnel during and after tunnelling. As a result, the soil profile along the tunnel alignment is *interpolated rather than directly measured* from data derived from a discontinuous set of borings and soundings, which are supplemented by knowledge of the geological history of the area. Therefore, small heterogeneities and irregular changes in soil properties are easily missed. Different layers have variable lateral extents and expressions, and only the most continuous layers can be identified from successive borings and/or CPTs. In sounding a layer, there is a lack of established criteria for identifying layer composition and recognizing the layer from contiguous CPT logs (Ngan-Tillard et al., 2003).

The main feature lacking in the standard soil- or site-investigation approach is a non-destructive technique that samples the tunnel trajectory before excavation. This task could potentially be performed with the seismic technique used in the oil and gas industry to detect hydrocarbons several kilometres below the surface. Such a technique makes use of waves reflected from the boundaries between contrasting layers that are detected at the surface. Removing undesired signals and focussing the data then provides a continuous image of both vertical and horizontal reflectors in the subsurface. Typically, compressional or P-waves are used; however, on-land surface-seismic techniques using P-waves have proved unsuccessful in imaging the first few tens of meters. For these cases, shear or S-waves are more suitable for imaging than P-waves, and some very successful profiles have been made from S-waves (Ghose, 2003). It is presumed that compressional waves are significantly influenced by pore fluids, while shear waves are mainly supported by the solid part of the soil and are therefore hardly influenced by the pore fluid. A combination of seismic information and data from

borings and soundings provides a reliable subsurface profile of the area. Ghose (2003) describes the integration of data from shallow shear-wave reflection and CPT data.

The above seismic technique can be employed from the surface or from the TBM. However, tunnelling commonly takes place in heavily urbanized areas where it is difficult to conduct a seismic survey from the surface. In such a setting, it makes more sense to use a seismic system located on the head of the TBM. Such a system would measure ground conditions along the tunnel alignment as the TBM advances. In hard rock, seismic prediction ahead of the tunnel face has been successful in providing information on abrupt changes in rock quality and the occurrence of formation boundaries (Kneib and Leykam, 2004). It would not be possible to obtain such information from seismic surveys at the surface. During the construction of the Tsukui Conduit Tunnel in central Japan, a horizontal seismic profiling system was employed (Inazaki et al., 1999). The firm Amberg Measuring Techniques developed a tunnel seismic system that uses reflected seismic waves around the tunnel. This system has been used in Japan, South Korea, and Sweden (Sattel et al., 1996). Kobayashi et al. (2003) describe a seismic reflection tomography system installed upon a TBM for the excavation of the Fujikawa Tunnel in Japan. Kneib et al. (2000) developed a seismic system located upon a TBM for use in soft soil. The system uses compressional waves and higher frequencies than those commonly used in existing surface-seismic techniques. One or two transmitters, and two or more receivers, are installed on the cutter wheel arms of the TBM. Such a system was also used during the construction of a tunnel in Duisburg-Meiderich, Germany (Falk, 1998).

The present paper demonstrates the way in which the seismic technique can be used to optimally image the area in front of a TBM. It is assumed that the sources only generate shear waves and that the receivers only detect shear waves. This is because shear waves are most suitable for imaging in soft soil. For imaging, we use optimal imaging operators that take advantage of the fact that the TBM is rotating and advancing laterally. Different models are created and analysed to assess the features the images can resolve, and to assess the way in which the resulting images can be used to detect obstacles.

2. The Seismic Technique from a TBM

In hydrocarbon exploration, advanced imaging techniques have been developed to image structurally complicated hydrocarbon reservoirs. Important issues in obtaining these images are the signal-to-noise ratio and the imaging or focussing of the reflected wavefield. Figure 1 provides a simple example in which a single source emits a wave that is diffracted by an obstacle (e.g., a boulder) and is then received by many sensors along a line in the depth direction. As shown in Fig. 1a, the recorded data as a function of time describes a hyperbola, while as a function of space they describe a point. Therefore, a focussing step is required to focus the energy to the point from which it originated: the obstacle. In geophysical jargon, this process is called seismic migration and involves the migration of the hyperbolic (depth, time) data to (depth, horizontal-position) data. The result of focussing is termed the image, as shown in Fig. 1b. It is evident that the resulting image is very good, although not perfect. The focussing, or seismic migration, was performed with a standard technique termed phase-shift migra-

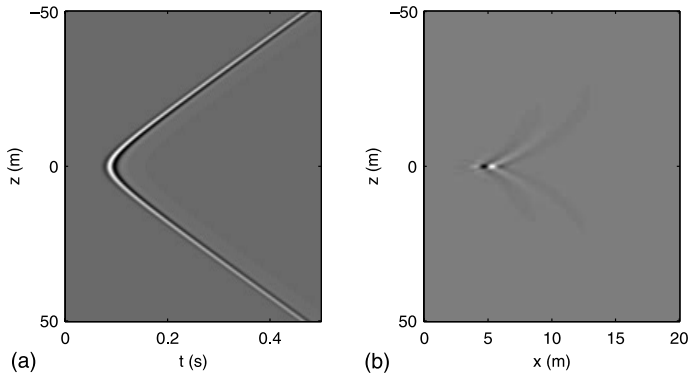


Fig. 1. Phase shift migration as used in the oil industry. The simulated data have a horizontal distance x to the boulder of 3 m and a vertical position z of 0 m: (a) recording in depth and time with 201 receivers; (b) imaged data in depth and horizontal position

tion. This technique assumes a planar layering of the earth and that receivers are suitably distributed with depth.

When using the above technique within a TBM configuration, the case is more complicated. In general, it is not possible to place transducers along a long line because space is only available on the TBM itself, or in the already excavated part of the tunnel. This limitation reduces the illumination of an obstacle in front of the TBM by

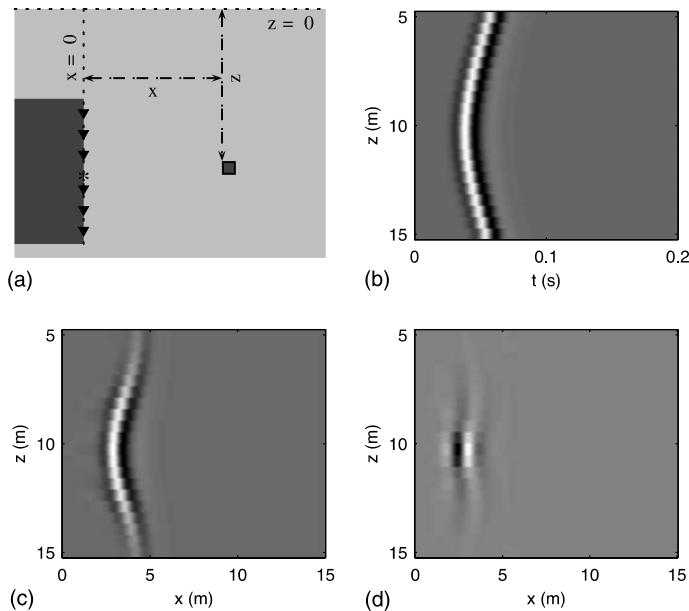


Fig. 2. Comparison of short-operator migration with migration used in the oil industry: (a) model with 21 receivers, boulder at lateral distance x and depth z ; (b) simulated data with distance $x=3$ m and depth $z=10$ m; (c) imaged data resulting from migration as used in the oil industry; (d) imaged data resulting from migration with short operators

seismic waves, especially toward the outer radius of the trajectory. The focussing operators used in the migration process in hydrocarbon exploration are truncated at the edges of the receiver array and generate errors when used in the tunnelling environment. Therefore, the configuration on the head of the TBM requires the adjustment of existing focussing methods. Figure 2 shows just how large the errors that arise from the above limitation can be. Because the space for receivers is limited by the diameter of the TBM, as shown in Fig. 2a, only a small part of the hyperbola is now registered, as shown in Fig. 2b. Focussing of the data using the standard technique then results in the image shown in Fig. 2c, which is clearly far from accurate. In this paper, new focussing operators that are especially adapted for tunnelling configurations are employed; the result of these operators is shown in Fig. 2d (a full discussion of this figure is provided in the following section). These new focussing operators are accurate and stable in a recursive focussing/migration scheme, and are derived using a weighted least-squares optimization. This paper focuses on the practical application of this focussing scheme. For theoretical considerations, the reader is referred to Swinnen (2003) and Thorbecke et al. (2004).

For the focussing step, the rotation and progression of the TBM towards an obstacle are typical aspects of a TBM configuration. This has advantages over the focussing step used in the oil industry. First, consider the effect of rotating the TBM. After one complete rotation, the TBM has moved forward only a few centimetres, which is a small distance compared with the resolution of shear waves in soft soil. This means that several measurements can be made during the rotation of the TBM while assuming an unchanged lateral position. Therefore, a large set of measurements can be made with only a limited number of sources and receivers. When taking into account that both the source(s) and receiver(s) are positioned at different distances from the TBM axis, an improved illumination of obstacles is achieved, thus providing an improved image. Rotation of the wheel is taken into account in the examples discussed herein, as is the effect of the lateral progression of the TBM. As the TBM advances and approaches the obstacle, the image is progressively improved because of improved illumination. The focussed result can be added to previous results, thereby increasing the quality of the image in terms of signal-to-noise ratio and resolution (mostly vertical). The closer the TBM approaches an obstacle, the better the image becomes. This feature raises the possibility of significantly improved image quality, as discussed later in the text.

3. Typical Configurations and Associated Focussed Images

This section considers typical configurations as encountered in practical tunnelling. For the TBM, a diameter of 10 m is assumed, with the TBM axis located 10 m below the ground surface. It is also assumed that the TBM is situated within a homogeneous soil with a typical shear-wave velocity for soft soils, i.e., 150 m/s. All models are studied in 2D conditions, with the source and receivers aligned vertically. This configuration rarely occurs in reality, but it may be a reasonable assumption when the cutter wheel is rotating. The frequencies emitted by the source are typical for shear waves (50 Hz centre-frequency). The datasets were generated using a finite-difference

scheme, and the full wavefield (including direct and reflected waves) was recorded. Many forward models use such a scheme (see Kneib and Leykam (2004) for more details). As the reflected wavefield is most important in these examples, the direct wavefield is calculated separately in a homogeneous model and subtracted from the full dataset.

3.1 Boulders

Consider again Fig. 2, where a boulder is situated in front of the centre of the TBM. The boulder is represented by a small square (1 m) in the grid, as used in the finite-difference modelling. To ensure simplicity of the model, the ground surface is not taken into account by assuming that the model continues to be homogeneous above the ground surface. When focussing data, the energy in the reflection hyperbola is migrated back to the position of origin. This should result in an image of the subsurface that contains the boulder, i.e., its position and size.

Following the traditional phase-shift migration shown in Fig. 2c, it is clear that a reflector exists in the subsurface in front of the TBM. However, little can be said about its size or vertical position. To improve the imaging result, the focussing techniques are adjusted to the situation specific for tunnelling. The traditional spatial focussing operators are very long, much longer than the diameter of the TBM. When applying these operators, they have no effect outside the diameter of the TBM. Consequently, the operators become unstable and generate errors that increase in images that are further from the TBM.

In the weighted least-squares algorithm, short extrapolation operators are designed to be accurate in terms of the operators from which they are derived, as well as being unconditionally stable in the focussing scheme. For each imaged point, a new operator is calculated such that the local background conditions can be taken into account. Applying these short extrapolation operators to the data processing shown in Fig. 2b produces the result shown in Fig. 2d. The difference between this new image and that shown in Fig. 2c, where long operators are used, is obvious. There are still some visible effects to the sides of the obstacle, which are caused by the limited number of receivers, but the maximum energy is now clearly limited to the location of the boulder itself.

Although only a limited part of the reflection hyperbola is registered in Fig. 2b, it does show a clear curvature, and the apex is easily determined. If the distance between the TBM and the boulder is increased, the hyperbola becomes flatter. This is evident in Fig. 3a and c, where the respective distances to the TBM have increased over the distance in Fig. 2b. With the limited number of receivers, it is even more difficult to image the energy of an almost flat reflection hyperbola. When focussing these data, as shown in the images in Fig. 3b and d, the horizontal position of the boulder is still easily determinable, but its vertical extension is less defined and the side effects from the limited recording aperture become stronger. However, even when the boulder is a large distance from the TBM, an estimate of its position and size can be determined. Clearly, the image of the boulder becomes more accurate as the TBM progresses toward it.

The effect of combining records during rotation of the cutter wheel is shown in Fig. 4. As discussed in the previous section, several recordings can be made during a single rotation of the cutter wheel. During this time, the TBM moves forward only a

Seismic Imaging from a TBM

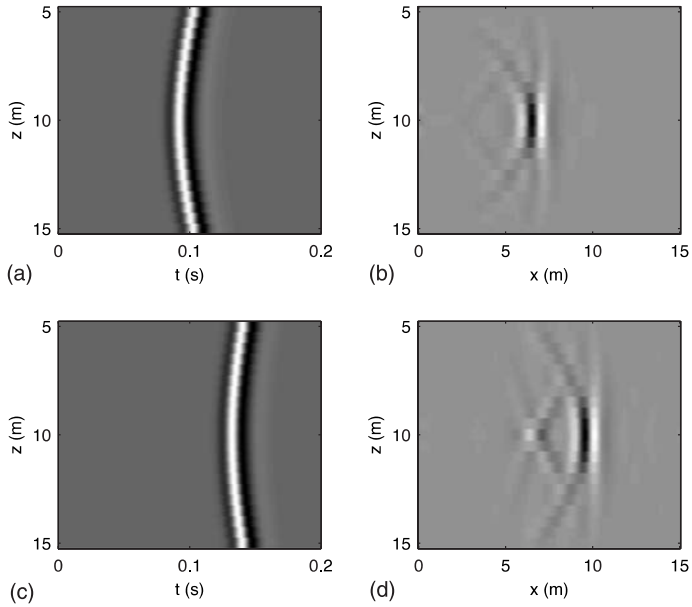


Fig. 3. Imaging of the boulder at different lateral distances from the TBM and depth $z = 10$ m: (a) simulated data with boulder at $x = 7$ m; (b) imaged data of (a); (c) simulated data with boulder at $x = 10$ m; (d) imaged data of (c)

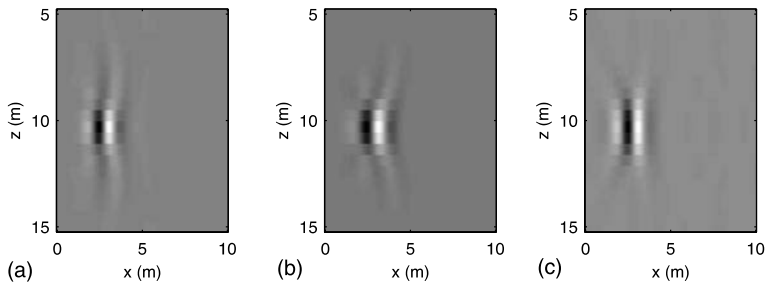


Fig. 4. Improvement in imaging resulting from the use of images derived from a “rotating” source and advancing TBM. The boulder is at $x = 3$ m and $z = 10$ m: (a) migrated data from single recording (non-rotating source, stationary TBM); (b) migrated data with summing for rotating source only, with source depth z varying from 7.5 to 12.5 m in steps of 0.5 m; (c) migrated data with summing for rotating source and progression of the TBM, with source depths varying as in (b) and distance x to boulder varying from 3 to 10 m in steps of 0.5 m

minimal amount; thus, the multiple recordings can be considered to have been taken at the same distance from the obstacle. Each recording still has the disadvantage of limited aperture and receivers, but the different recordings illuminate the boulder from different angles. Therefore, each recording contains different and complementary information. To take this into account under the assumed 2D conditions, the vertical position of the source is varied to simulate the rotating wheel of the TBM in 3D: receiver positions are not changed. The effect on the result can be seen in Fig. 4b. As

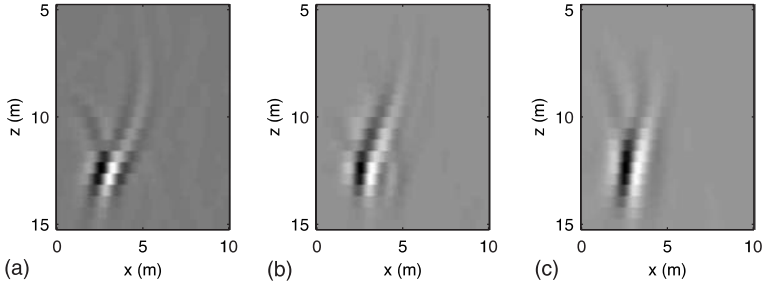


Fig. 5. Improvement in imaging resulting from the use of images derived from a “rotating” source and advancing TBM for a boulder below the TBM axis at distance $x=3$ m and depth $z=12.5$ m: (a) migrated data from single recording (non-rotating source, stationary TBM); (b) migrated data with summing for rotating source only, with source depth z varying from 7.5 to 12.5 m in steps of 0.5 m; (c) migrated data with summing for rotating source and progression of the TBM, with source depths varying as in (b) and distance x to boulder varying from 3 to 10 m in steps of 0.5 m

the boulder was already well imaged, the difference between the two figures is subtle. However, the side effects at the edges of the image have decreased in magnitude.

A second improvement can be made by combining images from different lateral TBM positions. In Figs. 2 and 3, it is evident that the influence of the limited aperture decreases as the TBM approaches the boulder. When combining images from different TBM positions, and taking into account the movement of the TBM, the energy of the boulder in each dataset coincides and is thereby multiplied. The noise or side effects are different in each shot and are therefore reduced in the process of combining the images. Using the same model as that used in Fig. 2, with a rotating source, an image was constructed over both a set distance and a varying distance between the TBM and the boulder. The result is plotted in Fig. 4c. The side effects around the image of the boulder have decreased further, and the vertical position of the boulder is now clearly resolved compared with that in Fig. 3.

As a variation on the previous model, the boulder is placed below the axis of the TBM in Fig. 5. Because of the asymmetry of the model, the lower part of the generated reflection hyperbola will be very short. This in turn will introduce larger artefacts into the image, as evident in Fig. 5a. The location of the image is accurate, but the side effects are stronger than those in the symmetric model, especially above the boulder. In Fig. 5b, the same boulder is illuminated by a vertical line of varying source positions, again simulating the rotating wheel of the TBM. The image is not appreciably improved compared with that in Fig. 5a. This lack of improvement can be explained by the relative position of the boulder and the sources. All sources illuminate the boulder from above. Therefore, they generate similar side effects that are not cancelled out when combining the separate images. This is not an exceptional situation given the limited area in front of the TBM. Adding the images that are generated while the TBM is progressing reduces the vertical extent of the artefacts, as evident in Fig. 5c. The boulder is now clearly resolved.

In the above examples, the ground surface is not taken into account because it is assumed that the boulder and the TBM are situated within an infinite homogeneous medium. Clearly, the ground surface influences the obtained data. The waves from both the source and the boulder are reflected by the ground surface and registered by

Seismic Imaging from a TBM

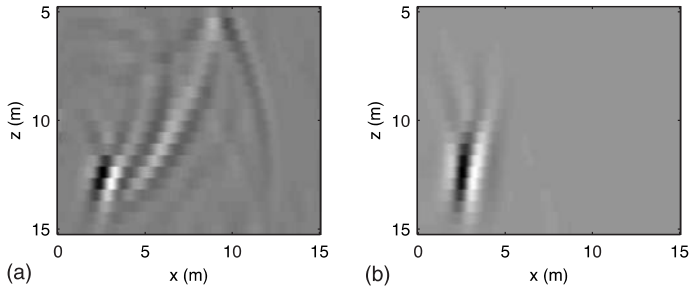


Fig. 6. Effect of ground surface on imaged data, with the boulder at distance $x = 3$ m and depth $z = 12.5$ m: **(a)** migrated data of single recordings (non-rotating source, stationary TBM); **(b)** sum of migrated data using “rotating” source and advancing TBM, with distance x to boulder varying from 3 to 10 m in steps of 0.5 m and depth z of source varying from 7.5 to 12.5 m in steps of 0.5 m

the receivers on the TBM. These reflected waves represent extra events in the data. Figure 6a shows the effect of such reflected waves on the imaged data with one source and the boulder situated below the axis of the TBM. The presence of the ground surface clearly increases the noise level in the migrated dataset. For the case of additional buried objects, interference of the additional reflections with other objects and with each other would result in a complicated image. Fortunately, reflections from the ground surface are not correlated with the focussing that involves multiple source positions. If the source moves either vertically or horizontally relative to the boulder,

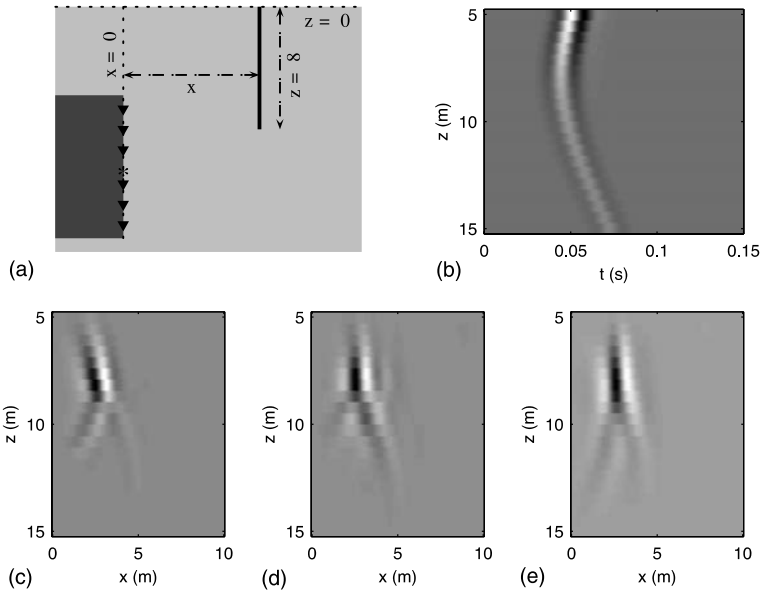


Fig. 7. Imaged data for a foundation obstacle: **(a)** model with a foundation obstacle from depth $z = 0$ to 8 m, with thickness of 0.5 m; **(b)** simulated data with foundation at distance $x = 3$ m; **(c)** migrated data from single recordings (non-rotating source, stationary TBM); **(d)** sum of migrated data of “rotating” source only, with source depth z varying from 7.5 to 12.5 m in steps of 0.5 m; **(e)** sum of migrated data of “rotating” source and advancing TBM, with source depths varying as in **(d)** and distance x to foundation varying from 3 to 10 m in steps of 0.5 m

the effect of the reflections in the data also changes. Therefore, these reflections do not coincide and are suppressed when combining recordings. This effect is evident when comparing Fig. 6b with Fig. 5c. The images are the same, and the effect of the ground surface is no longer visible. For the following examples in this paper, the medium is therefore considered infinitely homogeneous.

3.2 Foundation

The next model considers the case of a foundation (Fig. 7a). The foundation is assumed to extend vertically to a depth just above the TBM axis, with only part of the foundation in the path of the TBM. The simulated data are given in Fig. 7b, again showing a hyperbolic pattern. The figure shows that the slowest travel times are recorded at those receivers located at the same level as the foundation. At lower depths, the travel time increases and the amplitude of the reflection dampens rapidly. When these measurements are imaged in Fig. 7c, the result resembles the imaged data of the boulder in Fig. 5c. Therefore, it is difficult to determine if the object in front of the TBM is a boulder or a foundation. The bottom edge of the foundation is of course a strong diffraction point. However, amplifying the amplitude shows that there is no distinct reflection energy along the TBM axis.

Distinguishing between a boulder and a foundation is possible when the foundation is illuminated from different source positions. In Fig. 7d, measurements are combined from varying source positions, which simulate the rotating wheel of the TBM. Although the different source angles do not increase the energy level at the edge of the dataset, they do improve the depiction of the vertical extent of the foundation. The image is improved again in Fig. 7e, where the TBM approaches the foundation. The image shows an object with a greater vertical extent than that imaged in Fig. 5c. This example clearly shows the influence of the limited aperture of the receivers, which results in an area where no data can be imaged. When such data are interpreted, this limitation must be taken into account.

3.3 Inclined Beam

For the model shown in Fig. 8a, an inclined beam is situated entirely in front of the TBM. The lower end of the beam is below the TBM axis, while the top end is further from the TBM and located above the axis. The ends of the beam are strong diffraction points for the wavefield generated at the TBM (Fig. 8b). When this dataset is imaged, as shown in Fig. 8c, it initially appears that only a small obstacle is present in the subsurface. Diffraction from the lower end of the beam dominates over the energy recorded above the beam, and the image disappears upward.

When the source on the TBM moves to different vertical positions (Fig. 8d), it becomes evident that the event is generated by an inclined beam that extends above the TBM axis. The higher source positions act to increase the contribution of the top part of the beam, thereby making it visible in the image.

The effect of the diffraction points generated by the ends of the beam becomes stronger again when the horizontal progression of the TBM is taken into account (see

Seismic Imaging from a TBM

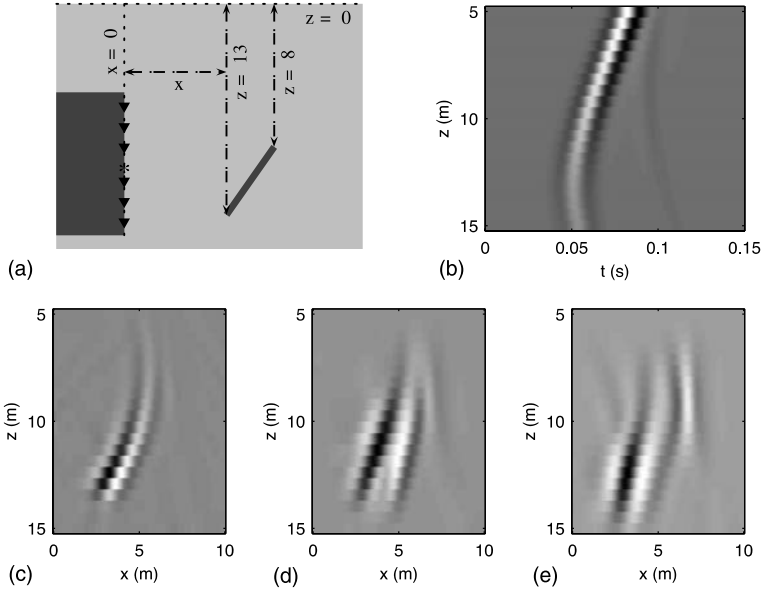


Fig. 8. Imaged data for a tilted beam obstacle: (a) model with tilted beam between $(x, z) = (x, 13)$ and $(x + 4, 8)$; (b) simulated data with tilted beam at horizontal distance $x = 3$ m; (c) migrated data from single recording (non-rotating source, stationary TBM); (d) sum of migrated data from “rotating” source only, with source depth z varying from 7.5 to 12.5 m in steps of 0.5 m; (e) sum of migrated data from “rotating” source and advancing TBM, with source depth varying as in (d) and distance x to tilted beam varying from 10 to 3 m in steps of 0.5 m

Fig. 8e). The lower end of the beam still dominates the image, but the diffraction of the upper end is now weakly visible. It is unclear from this image if a continuous obstacle is present in front of the TBM. However, during the excavation of the tunnel, both the measurements at one lateral position and the combined measurements from the progressing TBM are available. Together, they provide a clear indication of the shape of the obstacle.

3.4 Layered Medium

In reality, the TBM is never located in a completely homogeneous medium. In sedimentary settings, the subsurface is dominated by horizontal layering. The influence of such layering is investigated in the following two examples. Figure 9a repeats the model with the inclined beam in a two-layered situation. The soil in the top layer has the same velocity as before (150 m/s), while in the bottom layer the velocity is higher (200 m/s). The boundary is simulated as a gradual transition to avoid artefacts in the forward modelling that result from an abrupt change. Such gradual transitions are observed in nature. The simulated data in Fig. 9b are similar to those obtained for the single-layer situation. The reflection hyperbola is clearly registered sooner than that in the single-layer example because of the increased velocity of the bottom layer. Minor effects related to the layer transition are present in the data.

It is evident from Fig. 9c that the image from a single central source is not negatively affected by layering within the soil; however, only the lower end of the

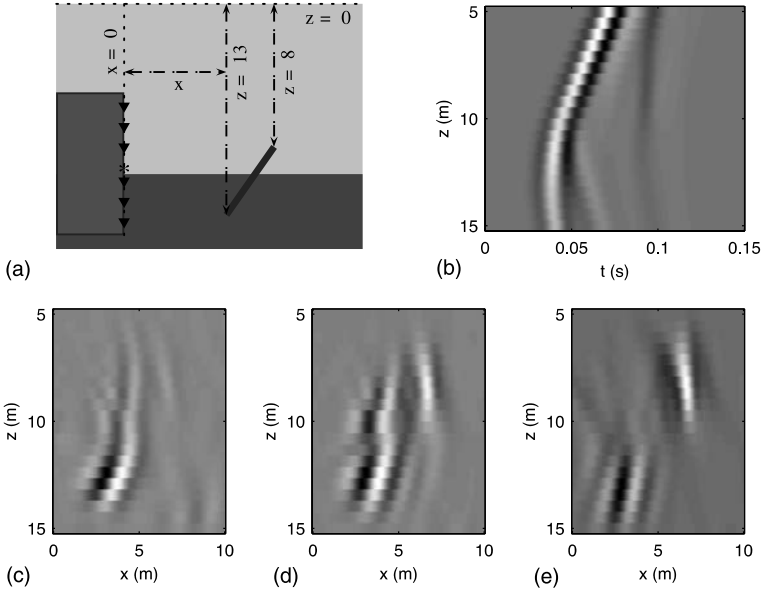


Fig. 9. Imaged data for a tilted beam obstacle within a double-layer setting: (a) model with tilted beam between $(x, z) = (x, 13)$ and $(x + 4, 8)$; (b) simulated data with tilted beam at horizontal distance $x = 3$ m; (c) migrated data from single recordings (non-rotating source, stationary TBM); (d) sum of migrated data from “rotating” source only, with source depth z varying from 7.5 to 12.5 m in steps of 0.5 m; (e) sum of migrated data from “rotating” source and advancing TBM, with source depth varying as in (d) and horizontal distance x to tilted beam varying from 3 to 10 m in steps of 0.5 m

obstacle is well defined. The result is similar to the single-layer situation. The influence of the layered medium is more apparent when a rotating source is modelled. Figure 9d shows a discontinuity around the TBM axis, and diffraction generated by the top end of the inclined beam appears in the data. This effect is more pronounced in Fig. 9e, in which images taken from the TBM as it moves toward the beam are combined. The image of the top end is stronger in this figure, although the imaged dataset can give the false impression of two small objects rather than a single beam. Therefore, a combination of different measurements will be necessary to resolve the obstacle.

To further examine the effect of layering on image acquisition, a vertical beam is considered an obstacle in the path of the TBM (Fig. 10a). The beam has the same vertical dimensions as the inclined beam described in the previous example. In the simulated data shown in Fig. 10b, the influence of the layered medium is clearly visible. The waves travel slower in the top part of the data, and a small artefact is generated at the layer transition. The data are migrated and combined in the same way as that in previous examples, with a fixed source (Fig. 10c), a “rotating” source (Fig. 10d), and both a “rotating” source and a progressing TBM (Fig. 10d).

Figure 10a to d shows the same effect: only part of the vertical beam in the top layer is visible. Although the energy in the lower beam is present, it is dominated by the top part; therefore, it is not apparent in the images. It has already been demonstrated for the inclined beam in Fig. 9e that the part of the beam situated in the slower

Seismic Imaging from a TBM

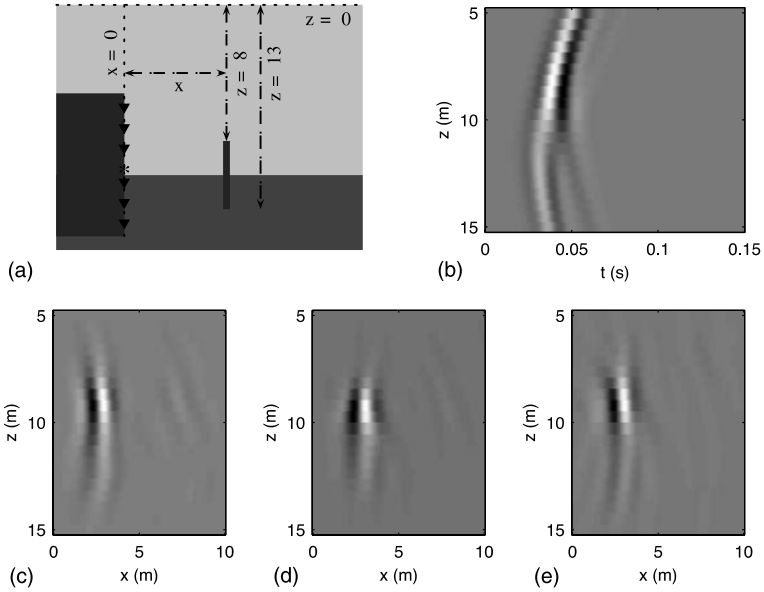


Fig. 10. Imaged data from a vertical beam obstacle within a double-layer setting: (a) model of vertical beam between depths $z = 8$ and 13 m; (b) simulated data with vertical beam at horizontal distance $x = 3$ m; (c) migrated data from single recordings (non-rotating source, stationary TBM); (d) sum of migrated data from “rotating” source only, with source depths z varying from 7.5 to 12.5 m in steps of 0.5 m; (e) sum of migrated data from “rotating” source and advancing TBM, with source depths z varying as in (d) and distance x to vertical beam varying from 3 to 10 m in steps of 0.5 m

soil layer is imaged more strongly. The longer travel path in the top part of the model acts to reduce the energy. Accordingly, both diffractions appear with similar energy. In the example with the vertical beam, all travel paths are equal and therefore the top part is more clearly imaged. If a longer part of the reflection hyperbola was measured in the data, the lower part of the beam would probably become stronger and the entire beam would be clearly visible.

4. Conclusions

In tunnelling applications, combinations of traditional geotechnical investigations and seismic surveys will provide better images of ground conditions along tunnel alignments. Existing seismic migration or focussing methods developed by the oil industry must be adjusted for the limitations of the tunnelling configuration where space for the source and receivers is limited.

This study uses short focussing operators that are optimized in a least-squares sense, and are accurate and stable. The use of these short operators greatly improves the accuracy of the image in front of the TBM. Furthermore, the special situation of the rotating cutter wheel and the horizontal progression of the TBM can be used to improve the image even further. In general, obstacles in the path of the TBM can be optimally imaged using the new focussing operators within both homogenous and layered media.

References

- Falk, C. (1998): Pre-investigation of the subsoil developments in construction of the 4th Elbe Tunnel Tube. *Tunn. Undergr. Sp. Tech.* 13(2), 111–119.
- Ghose, R. (2003): High-frequency shear-wave reflections to monitor lateral variations in soil, supplementing downhole geotechnical tests. *Proc. World Tunnelling Congress, Amsterdam, the Netherlands.*
- Inazaki, T., Isahai, H., Kawamura, S., Kurahashi, T., Hayashi, H. (1999): Stepwise application of horizontal seismic profiling for tunnel prediction ahead of the face. *Leading Edge*, 1429–1431.
- Kneib, G., Leykam, A. (2004): Finite-difference modelling for tunnel seismology. *Near Surface Geop.* 2(2), 71–93.
- Kneib, G., Kassel, A., Lorenz, K. (2000): Automatic seismic prediction ahead of the tunnel boring machine. *First Break* 18(7), 295–302.
- Kobayashi, T., Satou, J., Maeda, S., Yamamoto, T., Suguru, S., Honjou, T., Nishioka, K. (2003): New development of hard rock TBMs excavation monitoring tool and control system and true reflection tomography. (Re)Claiming the Underground Space, *Proc., of the ITA World Tunnelling Congress 2003, Amsterdam, The Netherlands*, 957–963.
- Sattel, G., Sander, B. K., Amberg, F., Kashiwa, T. (1996): Predicting ahead of the face-tunnel seismic prediction. *Tunnels and Tunnelling*, 24–30.
- Swinnen, G. (2003): *Acoustic Monitoring for Tunnel Boring in Soft Soils*. Delft University of Technology, The Netherlands, PhD Thesis.
- Thorbecke, J. W., Wapenaar, C. P. A., Swinnen, G. (2004): Design of one-way wavefield extrapolation operators, using smooth functions in WLSQ optimization. *Geophysics* 69(4), 1037–1045.
- Tillard, D. J. M., Maccabiani, J., Kruse, G., Kok, H., Weerts, H. (2002): A la recherche des empreintes laissées par les facies géologiques sur les profils pénétrométriques. *Journées nationales de géotechnique et de géologie de l'ingénieur*, Nancy, France, 1–11.
- Wermer, F. J. (1997): Second Heinenoord Tunnel – The first bored tunnel in the Netherlands. *Tunnels for People*, 411–416.

Authors' address: Gerd Swinnen, Faculty of Civil Engineering and Geosciences, Delft University of Technology, P.O. Box 5028, 2600 GA Delft, The Netherlands; e-mail: gerd.swinnen@skynet.be